Journal of Computational Acoustics

MOLECULAR DYNAMICS SIMULATIONS OF SOUND WAVE PROPAGATION IN A GAS AND THERMO-ACOUSTIC EFFECTS ON A CARBON NANOTUBE

MD AYUB[a,*], ANTHONY C. ZANDER[a], CARL Q. HOWARD[a], DAVID M. HUANG[b], BENJAMIN S. CAZZOLATO[a]

[a] *School of Mechanical Engineering,*
[b] *School of Chemistry and Physics,*
The University of Adelaide, Adelaide, SA 5005, Australia
[*] *md.ayub@adelaide.edu.au*

Received (2 July 2014)
Revised (Day Month Year)

Molecular dynamics (MD) simulations have been performed to study sound wave propagation in a simple monatomic gas (argon) and the thermo-acoustic effects on a single walled carbon nanotube (CNT). The objective of this study was to understand the acoustic behavior of CNTs in the presence of acoustic waves propagating in gaseous media. A plane sound wave was generated within a rectangular domain by oscillating a solid wall comprising Lennard-Jones atoms with the same intermolecular potential as the gas molecules. A CNT was aligned parallel to the direction of the flow at the wall at the opposite end of the domain. Interatomic interactions in the CNT were modeled using the REBO potential. The behavior of the sound wave propagation in argon gas without the CNT was validated by comparison with a previous study. The simulation results show that the thermo-acoustic behavior of CNTs can be simulated accurately using MD and that large-scale MD can be performed in the ultrasonic frequency range. This investigation will contribute to an improved understanding of the acoustic absorption mechanism of these nanoscopic fibers.

Keywords: Molecular dynamics simulation; sound wave propagation; carbon nanotube; nanoacoustics; nanoscopic absorption mechanisms.

1. Introduction

Mechanisms of sound absorption are currently well understood for conventional porous acoustic materials having fiber diameters or pores on the microscale (down to 1 μm). The relative influences of the various mechanisms are, however, expected to change for materials with pores or fibers at the smaller nanoscale (down to 1 nm), while other mechanisms and non-linear effects may also have a significant influence. In order to investigate the absorption mechanisms for nanoscale materials, the flow and acoustic propagation within and around a nanotube acoustic absorber will need to be modeled using analytical or numerical approaches appropriate to the nanoscale. The current research aims to implement an accurate and reliable simulation method to model the acoustic absorption mechanisms of carbon nanotubes (CNTs). Figure 1 exhibits a schematic of the modeling stage for aligned multiple nanotubes (CNT forest with millions of nanotubes per square centimeter grown on a silicon substrate), which shows a simplified representation of the physical system for

the interaction of sound waves within the tubes and also in between the tubes.

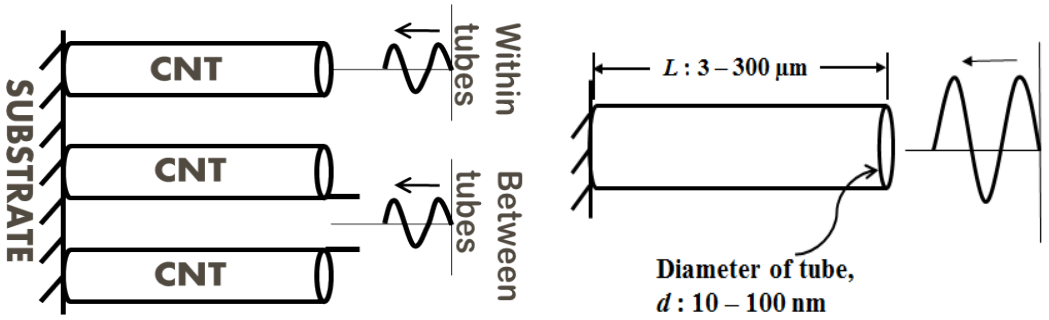

(a) Target modeling stage (b) Current modeling stage

Fig. 1: Schematics of the modeling to be undertaken showing (a) the arrangement of the multiple tubes for wave propagation (here 3 tubes are shown for illustration) and (b) the dimension scale of the nanotube and the current modeling stage for a single nanotube.

Wave propagation in micro- and nanoscale flows are usually characterized by the confinement of the fluid environment[1]. The hierarchy of the mathematical models available to solve such types of fluid dynamics problem can be categorised into two groups as continuum and non-continuum methods according to the varying degrees of approximation[2]. Quantification of the validity of continuum models and deviation from this behavior can be established by the Knudsen number, $Kn = \frac{\lambda}{H}$, which is a ratio of the molecular mean free path (λ) and characteristic length scale (H). For $Kn = 0$ to 0.001 the medium is considered to be in the continuum regime; for $Kn \geq 0.1$ the continuum approximation is considered to be invalid[1,3]. For the nanoscale structures considered in this research, acoustic waves propagate in air (a polyatomic gaseous media), and the flow is through cylindrical channel nanotubes. The relevant length scales that determine the Knudsen number are the average molecular free path of air at standard temperature and pressure (STP), which is 65 nm[4], and the nanotube diameter, which is around 50 nm. Thus, the characteristic scale for carbon nanotubes is comparable to the molecular mean free path, which indicates a transition flow regime, because the value of Kn will be in the range of 0.1 to 10 ($Kn = \frac{65}{50} = 1.3$). The large value of the Knudsen number for air flow in nano fibers indicates that particle-based non-continuum approaches should be implemented for the investigation of the flow behavior. As such, Molecular Dynamics (MD) has been identified as a suitable molecular method for the simulation of acoustic wave propagation at the nanoscale. A detailed review can be found in the authors previous articles[5,6] regarding the selection criteria for choosing the MD as an applicable method for this particular problem and the justification of those criteria against the most likely phenomena associated with the absorption mechanisms of nanoscale materials.

In this article, sound wave propagation in a simple gas is studied using a molecular method (Molecular Dynamics) and a preliminary investigation of the thermo-acoustic effect on a CNT is presented. Having a more complete understanding of the sound field inside an acoustic wave domain enables the simulation to be extended to the investigation of the CNT structural parameters controlling acoustic absorption. Simulations were initially performed for sound wave propagation in argon gas without CNTs present; thereafter it was extended to analyze the thermo-acoustic behavior of CNTs in the presence of acoustic wave propagation in a gaseous media. Simulations were conducted for high frequency sound in MHz to GHz range using a simple gas of limited number of molecules as the wave propagating media due to the limitations of computational expense. Simulation results were validated against the DSMC study[7] and compared with the theoretical estimation using the transmission matrix method[8].

2. MD Simulation of Sound Wave Propagation in a Monatomic Gas

Molecular simulations were performed for a plane sound wave propagating in a monatomic gas (argon) in a rectangular domain of length L_z as shown in Figure 2. The domain length was varied based on the acoustic wave frequency. An oscillating wall made of solid argon was used as a sound source and excited at $z = 0$ by imposing a sinusoidally varying velocity in the z-direction. The far end of the simulation domain was terminated by a reflecting wall, known as a specular wall, where the normal component of the particle velocity is reversed. In order to validate the MD results, the simulation domain was developed to resemble that of the DSMC study as reported by Hadjiconstantinou & Garcia[7].

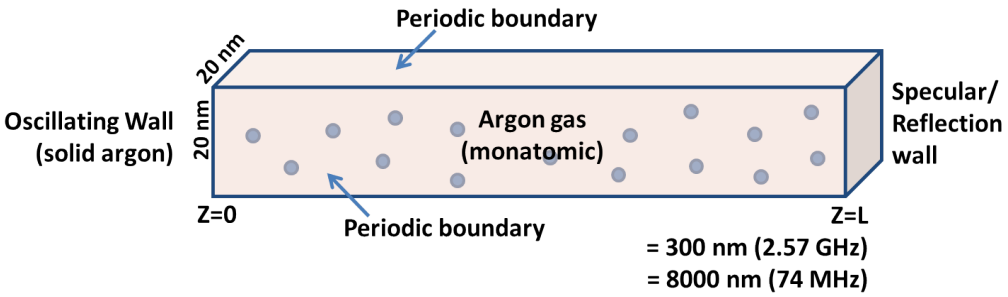

(a) Schematic of simulation geometry

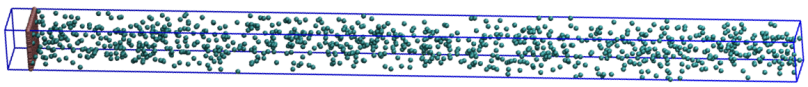

(b) Snapshot of the MD simulation domain

Fig. 2: Simulation domain and sound source model for acoustic wave propagation in argon gas.

The interactions between gas molecules (i.e., argon-argon) was described by a Lennard-Jones 12-6 type potential, U as[9]

$$U(r_{ij}) = 4\varepsilon_{ij}\left[\left(\frac{\sigma_{ij}}{r_{ij}}\right)^{12} - \left(\frac{\sigma_{ij}}{r_{ij}}\right)^{6}\right] \tag{1}$$

where r_{ij} is the intermolecular distance between atoms i and j, and ε_{ij} (= 10.33 meV) and σ_{ij} (= 3.40Å) are the Lennard-Jones parameters for argon molecules[9]. The intra-atomic interactions between the oscillating wall atoms (solid argon) were also expressed with the same potential parameters as the gas molecules. The cut-off distance for the LJ function was set to 3σ for the interactions of the gas and wall molecules. A short range purely repulsive WCA (Weeks-Chandler-Andersen) potential[10] was introduced for the interaction between the argon atoms of the solid wall and those of the propagating media (gas) by truncating the Lennard-Jones potential at the $2^{\frac{1}{6}}\,\sigma_{ij}$.

The wall oscillates harmonically in the z-direction with displacement Z_w and oscillation speed $V_w(t)$ as a function of time t according to

$$Z_w(t) = a(1 - \cos\omega t) \tag{2}$$

$$V_w(t) = a\omega \sin\omega t \tag{3}$$

where the displacement and motion of the wall is characterized by the amplitude a and the angular frequency ω. The sound source yields a plane sound wave propagating in the z-direction leading to a velocity variation

$$v_i(z,t) = v_0 \exp\left[i(\omega t - kz) - mz\right] \tag{4}$$

with the maximum gas velocity $a\omega$, which corresponds to the peak velocity of the oscillating wall, $v_0(= a\omega)$; where $k = \frac{2\pi}{l}$ is the wavenumber with l being the acoustic wavelength and m is the attenuation coefficient. Due to the specular wall at the far end of the domain, the propagating wave will be reflected at the termination as

$$v_r(z,t) = -v_0 \exp\left[i(\omega t - k(2L - z) - m(2L - z)\right] \tag{5}$$

Superposition of the incident and reflected waves leads to a standing wave of the form[11,7]

$$v(z,t) = A(z)\ \sin\omega t + B(z)\ \cos\omega t \tag{6}$$

where

$$A(z) = v_0\ [e^{-mz}\ \cos kz\ -\ e^{-m(2L-z)}\ \cos k(2L - z)] \tag{7}$$

$$B(z) = -v_0\ [e^{-mz} \sin kz\ -\ e^{-m(2L-z)}\ \sin k(2L - z)] \tag{8}$$

$A(z)$ and $B(z)$ are the components of the velocity amplitude of the standing wave which can be extracted from the numerical solution based on a method used by Hadjiconstantinou

and Garcia[7]. In order to calculate the velocity components, i.e. $A(z)$ and $B(z)$, from the simulation results, the instantaneous velocity $v(z_{jj}, t_{ii})$ of the gas molecules in a number of bins/slices perpendicular to the z-axis along the box length is recorded at each time step after the initial transient has passed. Here, z_{jj} is the position of the bin and t_{ii} is the recorded time step with $jj(= 1, 2, 3.....M)$ being the bin number index and $ii(= 1, 2, 3.....N)$ the time sample index. Thereafter, a least-square method is used to evaluate $A(z)$ and $B(z)$ from the recorded data. Detailed equations can be found in Hadjiconstantinou and Garcia[7]. A non-linear fit of Eqs. (7) and (8) to the numerical solution of $A(z)$ and $B(z)$ is performed using the Nelder-Mead simplex method to estimate the wave number k and the attenuation coefficient m. A phase shift is included in the wave equations for the parameter fits for theoretical prediction at higher frequencies in the range of GHz due to the entrance effects near to the sound source[7].

2.1. *Simulation Details*

Molecular dynamics (MD) simulations were carried out for acoustic wave propagation at two different frequencies of 67 MHz and 2.57 GHz, as required for validating against the DSMC results[7]. The large-scale atomic/molecular massively parallel simulator (LAMMPS) package[12] was used for MD simulations. A simulation domain with transverse dimensions $L_x = L_y = 20$ nm (2.57 GHz), 12 nm (67 MHz) was modeled with the domain length L_z being chosen to be no longer than a few wave lengths ($L = \frac{7}{4}l$) to reduce the simulation cost. Domain lengths of 300 nm and 8000 nm were used for simulating acoustic wave propagation at the frequencies of 2.57 GHz and 67 MHz, respectively. The periodic boundary condition (PBC) is considered at each face of the simulation domain in directions perpendicular to the propagating wave. The time step of the simulation was taken to be 1 fs, which corresponds to the numerical integration time step Δt of Newton's equation of motion for argon as[13],

$$\Delta t = 0.0005\sigma\sqrt{\frac{M_m}{\varepsilon}} \tag{9}$$

where M_m is the molecular mass, and σ and ε are the parameters for LJ potential. This choice of time step also satisfies the time step constraints suggested by Hadjiconstantinou and Garcia[7] for accurate molecular simulation and to capture the time evolution of the wave profile, that is, the time step should be significantly smaller than the mean collision time ($\ll \frac{\lambda}{c_m}$) and the characteristic time ($\ll \frac{2\pi}{\omega}$), with $\lambda(=7.24\times10^{-8}$ m) being the mean free path and c_m being the most probable velocity. Here, $c_m=\sqrt{\frac{2k_BT}{M_m}}$, k_B is the Boltzmann constant and T is the gas temperature.

Simulations were initiated with a uniform distribution of gas velocity and were equilibrated at atmospheric temperature, $T = 273$ K and pressure, $P = 1$ atm with the gas density of argon being $\rho = 1.8$ kgm^{-3}. An initial velocity amplitude of the sound source was chosen to avoid nonlinear effects in the wave propagation, such as shock formulation, by ensuring that viscous terms dominate nonlinear terms[11,7], i.e. when Reynlods number,

$Re \ll 1$, then

$$v_0 \ll \frac{\omega\mu}{\rho c} \tag{10}$$

where μ is the viscosity and c is the classical sound speed. This criterion can also be expressed as $v_0 \ll \frac{c}{R}$, where $R = \frac{c^2\rho}{\omega\mu}$ is the acoustic Reynolds number[7]. In the MD simulations, the velocity amplitude of the sound source was chosen to be $v_0 = 0.025c$ at the lower frequency of 67 MHz ($R \approx 20$) and a larger initial amplitude of $v_0 = 0.15c$ was used at the higher frequency of 2.57 GHz ($R = 0.5$) as the acoustic wave was damped significantly due to the large attenuation at this frequency. However, v_0 is assumed to be smaller compared to the most probable molecular velocity c_m of the gas, which usually has the same order as the sound speed c.

2.2. *Numerical Results and Validation*

To evaluate $A(z)$ and $B(z)$, the sampling was started at a point where the change of velocities becomes relatively small, i.e. at a steady state condition of the flow. In order to determine the starting point for sampling, a monitor point was set to observe the change of velocities at each moment of an integer period of the propagating wave. Additionally, the simulation conditions were also monitored for sanity checking of the gas temperature and pressure fluctuations during the wave propagation. Figure 3 shows the harmonic oscillations of the mean spatial gas temperature and the gas pressure during the acoustic wave propagation at a frequency of $f = 67$ MHz ($R \approx 20$). As shown in Figure3a, the maximum increase of mean temperature due to dissipation was less than 2%, hence the change of sound speed is less than 1.5% since the sound speed varies as $\sqrt{T}$ [7].

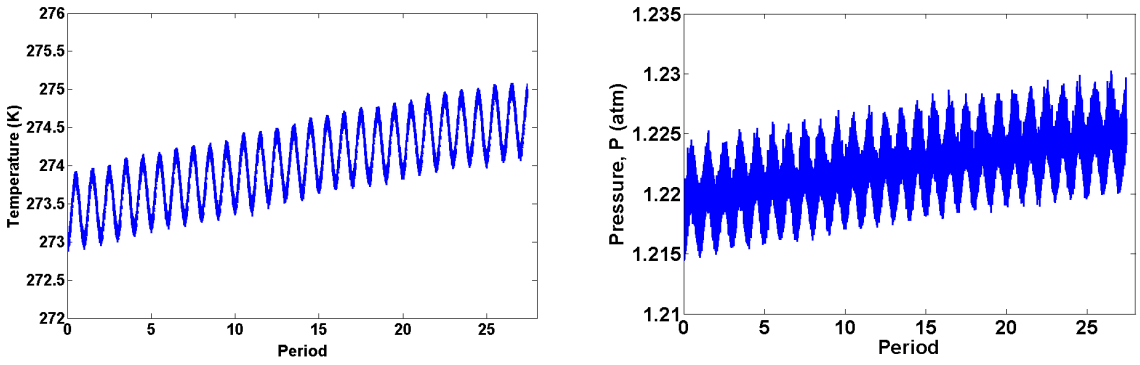

(a) Mean spatial gas temperature

(b) Mean spatial gas pressure

Fig. 3: Mean spatial temperature and pressure oscillations of the gas for frequency, $f = 67$ MHz ($R \approx 20$).

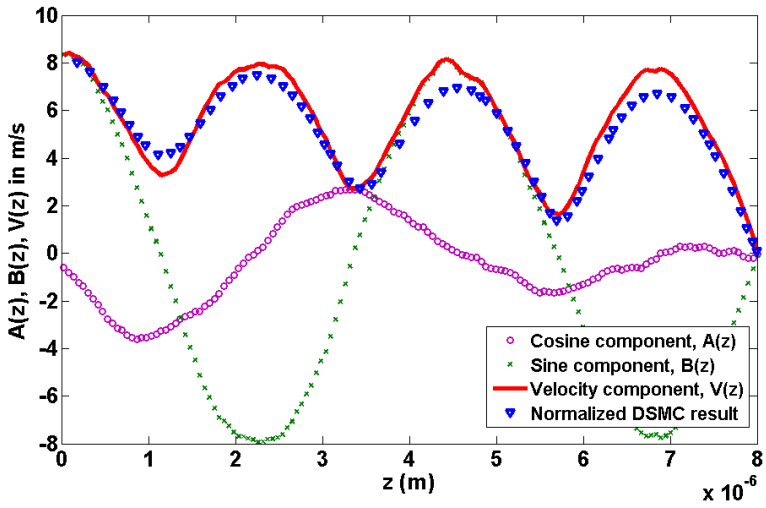

Fig. 4: Velocity amplitude $V(z) = \sqrt{A^2 + B^2}$ as a function of distance for frequency, $f = 67$ MHz ($R \approx 20$). Normalized DSMC result is plotted against the MD simulation result.

After the transient period has passed, sampling was done from 15 periods to 27 periods, with 45 time samples in each period and 80 spatial bins per wavelength at a frequency of $f = 67$ MHz. Numerical estimation of the cosine and sine components, $A(z)$ and $B(z)$, of the velocity amplitude is presented as a function of distance z in Figure 4. A comparison between the MD results and the normalized DSMC[7] results of the velocity amplitude $V(z) = \sqrt{A^2 + B^2}$ is also displayed. It can be seen that the MD results match very well with the normalized DSMC results despite the discrepancy near the acoustic source. This discrepancy can be attributed to the number of sample averaging, which indicates the simulation is needed to be run for further longer periods to achieve better averaging.

For the validation of MD results at higher frequencies, simulations were performed at frequency $f = 2.57$ GHz for an acoustic Reynolds number $R = 0.5$. A challenge of simulation at higher frequency is that the rapid oscillation of the sound source heats the system very quickly as the acoustic source continuously does work on the gas. Therefore, an auxiliary mechanism that is compatible with wave propagating modeling was required to remove the additional heat from the system. A Noose-Hover thermostat (NVT) was coupled loosely with the system in directions perpendicular (x and y) to the propagating wave to control the increasing temperature. It was observed that the thermostatting with a damping time of 5 periods of the acoustic frequency can effectively control the temperature increase. Effects of the thermostatting damping time on the propagating wave are elaborated in Appendix A. Figure 5 shows the harmonic oscillations of gas temperature and gas pressure during the acoustic wave propagation at $f = 2.57$ GHz ($R = 0.5$). As shown in Figures 5a and 5b, the maximum increase of mean temperature and pressure were kept to less than 5% of its

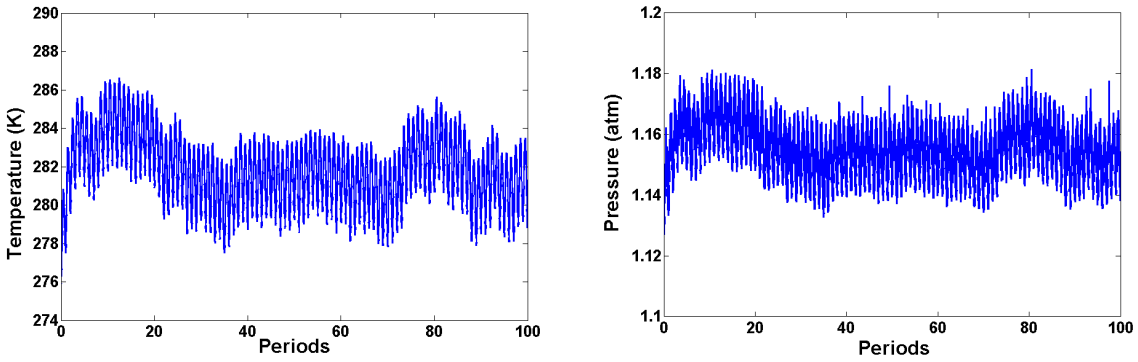

(a) Mean spatial gas temperature

(b) Mean spatial gas pressure

Fig. 5: Mean spatial temperature and pressure oscillations of the gas for frequency, $f = 2.57$ GHz ($R = 0.5$).

equilibrated temperature and pressure, hence the change of sound speed is less than 2.5%, which also indicates a higher temperature variation due to dissipation at this frequency.

To extract the cosine and sine components, $A(z)$ and $B(z)$, of the velocity amplitude at higher frequency, sampling was done between 70 periods to 100 periods, with 60 spatial bins in each wavelength. Figure 6a shows the comparison between the normalized DSMC data and MD results for $A(z)$ and $B(z)$. Normalization of the DSMC data of the simulated component of the velocity amplitude shows good agreement with the MD results. In the previous analyses[7,14,15], it was found that the free molecular flow at higher frequency dominates near the acoustic source in the region smaller than one mean free path (λ). This effect was verified by applying a nonlinear fit to the cosine and sine components of the velocity amplitude, a similar method used by Hadjiconstantinou and Garcia[7], and restricting the fit to either one mean free path ($z>\lambda$) or a half mean free path ($z>0.5\lambda$). Figure 6b shows that both restrictions give a better fit to the waveforms model for a constant value of sound speed and attenuation coefficient at domain length larger than one mean free path; however the waveforms do not fit very well near to the acoustic source in the region $0<z<\lambda$. This results verifies the observation made by Hadjiconstantinou and Garcia[7] that the free molecular flow is important near to the source at domain length smaller than one mean free path. Unknown parameters, such as the sound speed (c) and attenuation coefficient (m) for the sound wave propagation in a monatomic gas, were also obtained using the nonlinear fitting of the waveforms to the simulated data. Extracted values for sound speed (c) and attenuation coefficients (m) are 494 ms^{-1} and 1.35×10^7 m^{-1}, which are similar to the predictions by the DSMC method.

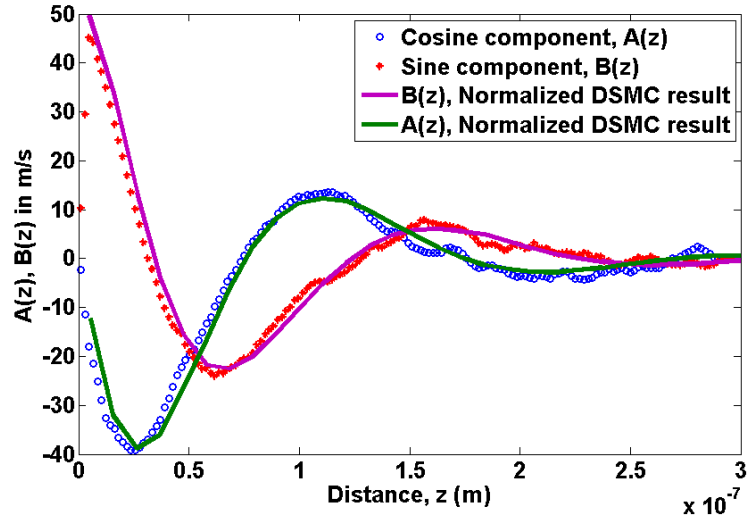

(a)

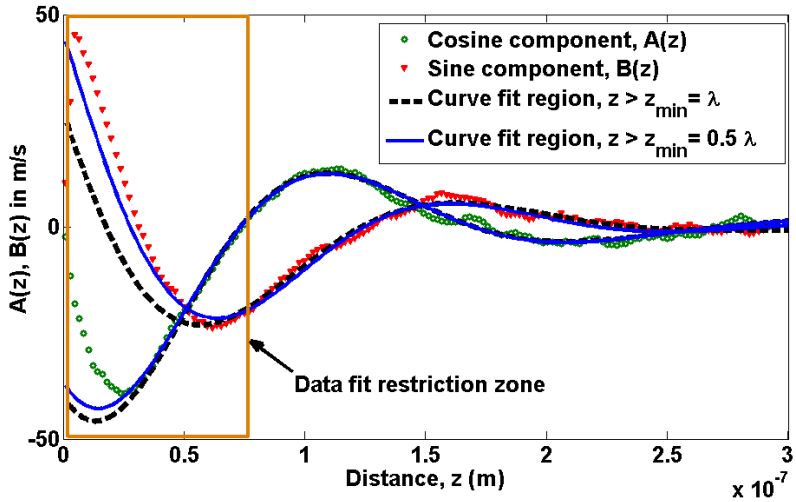

(b)

Fig. 6: Cosine and sine components, $A(z)$ and $B(z)$ of the velocity amplitude as a function of distance for frequency, $f = 2.57$ GHz ($R = 0.5$). (a) Normalized on DSMC result plotted against the MD simulation result. (b) Curve fit to cosine and sine components of velocity amplitude as a function of distance.

Based on the above discussions and validation results, it can be concluded that the MD simulation results are consistent with the results of previous molecular simulations, such as the DSMC method, for sound wave propagation in a gas, and the MD method can be effectively used to model acoustic wave propagation.

3. Theoretical Comparison with Transmission Matrix Method of Duct Systems

The transmission matrix method described by Beranek and Ver[8] for the analysis of duct systems with plane waves can be used to make a theoretical comparison with the simulation results. A few modifications were made to the transmission matrix equations for a duct system with uniform cross section in order to adapt the method for the current simulation domain. A complex wave number $K = k - im$, was considered instead of the classical wave number k to include the attenuation term m in the wave equation. In addition, k_c is replaced with K, assuming no frictional energy loss along the simulation domain. The acoustical pressure, p_j, and mass velocity field, $\rho S v_j$, at the j-th location in the simulation domain can be obtained by (see Beranek and Ver[8], p377),

$$\begin{bmatrix} p_j \\ \rho S v_j \end{bmatrix} = \begin{bmatrix} T_{11}\ T_{12} \\ T_{21}\ T_{22} \end{bmatrix} \begin{bmatrix} p_0(z=0) \\ \rho S v_0(z=0) \end{bmatrix} \tag{11}$$

where S is the cross section of the simulation domain and the transmission matrix is given by (see Beranek and Ver[8], p377),

$$\mathbf{T} = \begin{bmatrix} T_{11}\ T_{12} \\ T_{21}\ T_{22} \end{bmatrix} = \begin{bmatrix} \cos(KL_j) & i\frac{c}{S}\sin(KL_j) \\ i\frac{S}{c}\sin(KL_j) & \cos(KL_j) \end{bmatrix} \tag{12}$$

Figure 7 shows the comparison between the transmission matrix results and the MD simulation results. It can be seen from Figure 7a that the MD simulation results show good agreement with the theoretical estimation of velocity amplitude at lower frequency. Whereas, at higher frequency, it exhibits a consistent agreement of the curve at domain length larger than one mean free path ($z > \lambda$) and does not compare well near to the acoustic source at length smaller than one mean free path. This indicates that the aforementioned effect of free molecular flow is still important for higher frequency and linear acoustic theory is not applicable near to the source at this frequency.

4. MD Simulation of CNT in the Presence of Acoustic Wave

A preliminary investigation for the acoustic wave propagation in the presence of a nanomaterial is presented in this section as part of the study of sound wave propagation using molecular dynamics. This is an extension of the previously validated simulation to include of a carbon nanotube (CNT). The focus of the study is on single-walled CNTs (SWCNT) as a representative nanoscopic fiber for acoustic absorption purposes. MD simulations were performed to capture the atomistic processes involved in the interaction between the acoustic wave and the CNT, which govern the energy transfer between them and control the acoustic absorption. The simulation domain was modeled with a CNT aligned parallel to the direction of the flow at the wall at the opposite end of the domain to the acoustic source. A schematic of the simulation geometry and a snapshot of the simulation domain

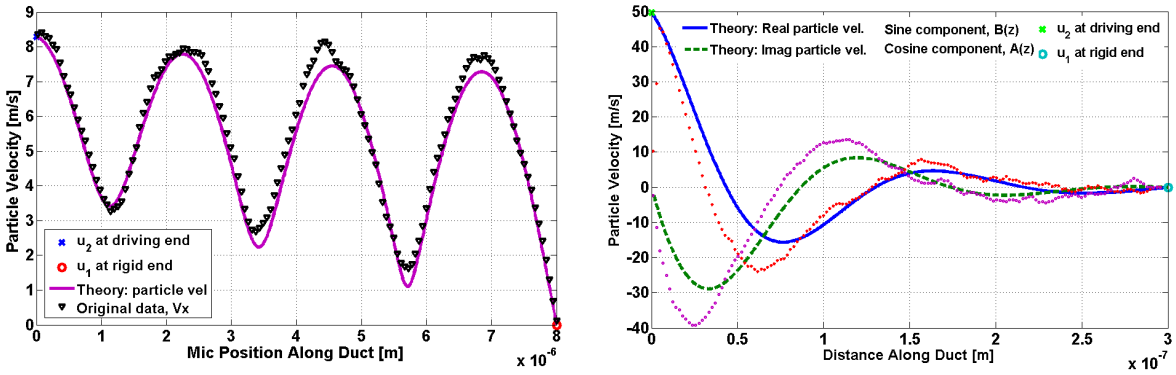

(a) R≈20 (b) R=0.5

Fig. 7: Comparison of the MD simulation results with theoretical estimation using transmission matrix method. (a) Velocity amplitude $V(z) = \sqrt{A^2 + B^2}$ as a function of distance for frequency, $f = 67$ MHz ($R \approx 20$). (b) Cosine and sine components, $A(z)$ and $B(z)$ of the velocity amplitude as a function of distance for frequency, $f = 2.57$ GHz ($R = 0.5$).

are shown in Figure 8. Simulation was carried out for high frequency sound wave propagation at frequency $f = 2.57$ GHz to reduce the computational cost. Additionally, the domain length was reduced to the order of one wavelength in order to ensure that the propagating wave was of sufficient amplitude at the termination wall, based on the consideration of the relatively large attenuation at this frequency. Furthermore, it should also be reemphasized that at the high frequency considered, i.e. $R = 0.5$, simulations were performed with a large initial velocity amplitude due to the considerable attenuation. As described earlier, the wave velocity amplitude of $v_0 = 0.15c$ was used to ensure that the sufficient signal amplitude existed within the curve fit region (z $>0.5\lambda$).

4.1. *Simulation Details*

An open-end (uncapped) (5,5) SWCNT of length $L_{CNT} = 25$ nm and diameter $d_{CNT} = 0.69$ nm was cantilevered and immersed in a simulation domain of gaseous argon with a density of 1.8 kg m^{-3}. In the simulations, one end of the CNT, i.e., atoms within 0.1 nm of the clamped boundary, is fixed and the reminder of the CNT atoms were set to move freely according to the interaction forces on them following Newtonian motions. The simulation domain has dimensions similar to that of the validation case, i.e., $L_x = L_y = 20$ nm in the transverse direction and $L_z = 150$ nm in the flow direction, as illustrated in Figure 8. The domain size was large enough to exclude the inter- nanotube short-range coupling interactions with the source. Hence, the simulations conducted here with a periodic boundary condition on the side walls of the domain represent an array of nanotubes with an area density of 0.0025 nm^{-1}. A second generation REBO[16] (Reactive Empirical Bond Order) potential was used to express the inter-atomic interactions between carbon atoms (carbon-

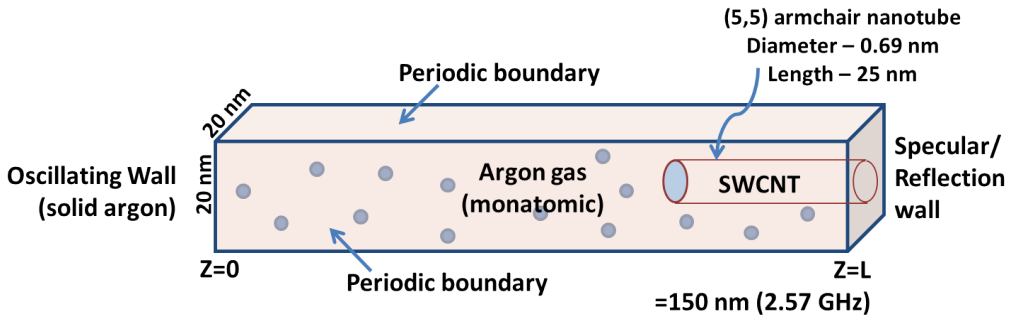

(a) Schematic of simulation geometry

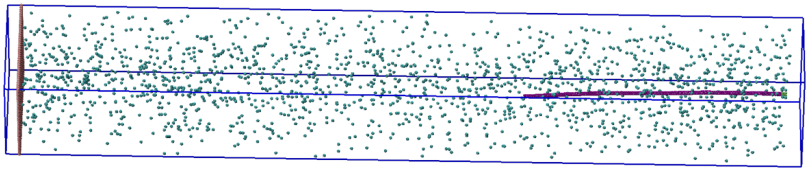

(b) Snapshot of the MD simulation domain

Fig. 8: Simulation domain and sound source model for acoustic wave propagation in argon gas with the immersed CNT.

carbon) in the CNT. The interactions between argon and carbon atoms (argon-carbon) were represented by a Lennard-Jones potential with parameters ε_{Ar-c} (= 4.98 meV) and σ_{Ar-c} (= 3.38 Å)[9]. Similar to the validation case, the oscillating wall and wave propagating media were modeled using solid and gaseous argon, respectively. The total number of molecules in the simulation domain, $N_{wall} = 2965$, $N_{argon\ gas} = 1792$ and $N_{CNT} = 2040$, were conserved owing to the periodic boundary condition.

Simulations were performed with a time step size of 0.5 fs using a velocity-varlet algorithm. The gas molecules and CNT are thermalized to 273 K at 1 atm with a uniform distribution of the gas velocity and then maintained for 12.5 ns using a Langevin thermostat in an NVE ensemble to equilibrate the argon gas and their interactions with the CNT. Thereafter, simulation conditions during acoustic wave propagation were maintained by a NVT thermostat which was loosely coupled with the gas in the direction perpendicular to the propagating wave. The change of velocity was monitored during the wave propagation at a monitoring point $z = 79.8$ nm, yielding the profile shown in Figure 9. As the flow reached the steady state, i.e, after 70 periods, sampling was done from 70 periods to 100 periods.

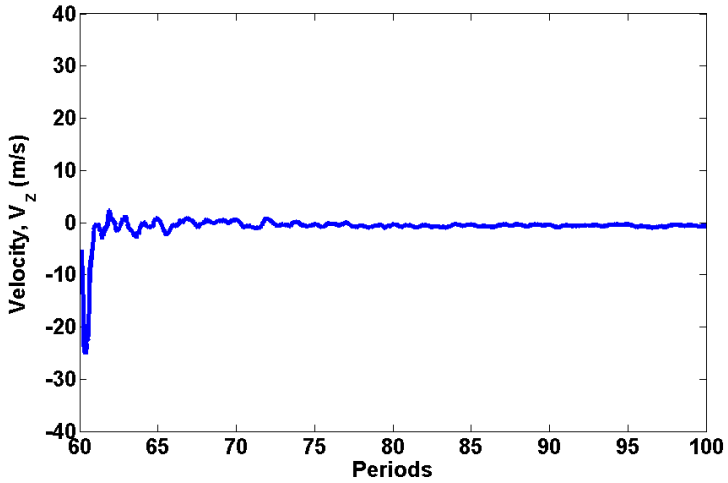

Fig. 9: Velocity change at monitoring point, $z = 79.8$ nm.

4.2. *Results and Discussion*

The variation of the mean spatial gas temperature and gas pressure during the wave propagation was closely monitored to check the effect on sound speed due to dissipation. Figure 10 shows the change of gas temperature and pressure as a function of the integer period of the propagating acoustic wave. The maximum increase in the temperature and pressure of the gas was less than 5%, which confirms that the change of sound speed is less than 2.5%.

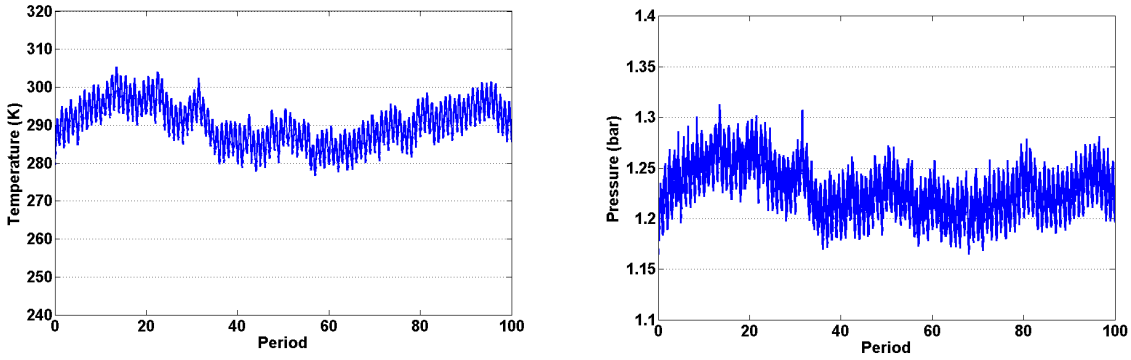

(a) Mean spatial gas temperature

(b) Mean spatial gas pressure

Fig. 10: Mean spatial temperature and pressure oscillations of the gas for frequency, $f = 2.57\,GHz$ $(R = 0.5)$.

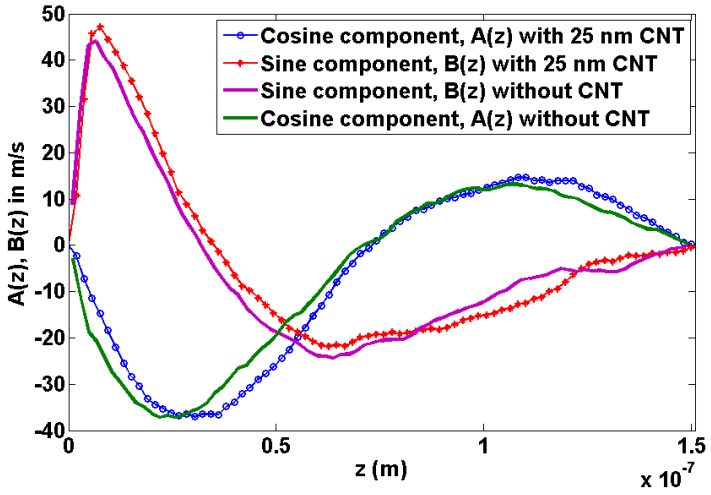

Fig. 11: Sine and cosine components of velocity amplitude as a function of distance in a simulation domain with and without CNT

Additional simulations were performed for sound wave propagation without the CNT present for the same domain dimensions and conditions. The results were utilized to obtain a comparison of velocity components ($A(z)$ and $B(z)$) with and without the CNT present, as exhibited in Figure 11. This comparison was made in order to observe the acoustic damping due to the effect of fluid-structure interaction between the gas and the CNT, induced by the acoustic wave. It can be seen that the components of the velocity amplitude in the presence of CNT show a small but discernible change in the velocity profile compared to that of the domain without CNT, which are induced due to the interaction between the acoustic wave and the CNT. The results in Figure 11 reveal a discontinuity in the cosine and sine components around the free end of the CNT at $z = 125$ nm, and a shift of the curves relative to those obtained without the CNT present. Curve fitting of the waveform components over the entire domain is no longer appropriate because there are two coupled domains: one between the source and the tip of the CNT which contains only argon atoms; and another for the reminder of the domain which contains both argon and a CNT. Further analysis would be required to develop suitable method to predict the acoustic absorption due to the presence of the CNT from the numerical results.

The change in temperature and kinetic energy of the CNT were simultaneously monitored to check the thermo-acoustic effect on the CNT. Figure 12 shows the time history of temperature and kinetic energy of the CNT during the wave propagation. The results show that the CNT does not have significant thermo-acoustic fluctuations harmonically coupled with the gas, which may indicate weak coupling of fluid-structure interactions during the wave propagation. In addition, the differences of heat transfer rate (frequency) as

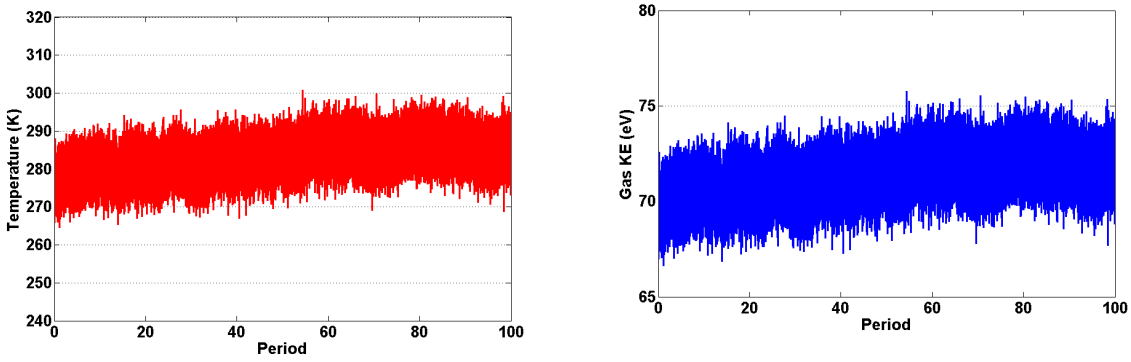

(a) Mean spatial temperature of CNT (b) Kinetic energy of CNT

Fig. 12: Change of temperature and kinetic energy of CNT as a function of time.

well as physical coupling mechanism involved between polyatomic (CNT) and monatomic molecules (argon) may also be a reason for there not being a strong coupling of thermo-acoustic fluctuations with CNT temperature.

The vibrational behavior of the CNT was also analyzed to investigate any significant changes in its structural modes. Although no considerable changes are observed in the velocity amplitude of the propagating wave and the temperature and kinetic energy of CNT, visualization of the MD simulation using VMD (Visual Molecular Dynamics) shows several CNT structural modes of vibration. To gain further insight into the excitation of structural vibration in the CNT, a principal component analysis (PCA) is performed for the last 40 periods of simulations without (equilibration) and with excitations (acoustic wave), for the atomic trajectory $z_i(t)$, where $i = 1, 2, ...3N$, where N is the total number of atoms[17]. The results of the PCA are presented in the scree plot for CNT vibration modes as shown in Figure 13. As can be seen from Figure 13, for both cases with and without excitations, there are no considerable changes in the most dominant vibrational modes.

However, it was observed that the deflection amplitude and energy of the CNT are amplified with acoustic excitation compared to that of the case without the excitation, which can be verified from examination of the recorded deflection of the tip (as illustrated in Figure 14). The displacement of the CNT tip, its thermal fluctuation amplitude and kinetic energy were recorded during the simulations. Results for both without and with acoustic wave excitation are plotted in Figure 15. As displayed in Figure15a, when no acoustic wave is driving the system, i.e. when the system is in its equilibration state, the position of the CNT tip oscillates around its original position $d(x_i) = \mathrm{d}_0(t = 0)$ with a standard deviation of amplitude $a = 0.383$ nm. This oscillation can be regarded as thermally induced motion attributed to both the excitation of phonon modes in the CNT and the

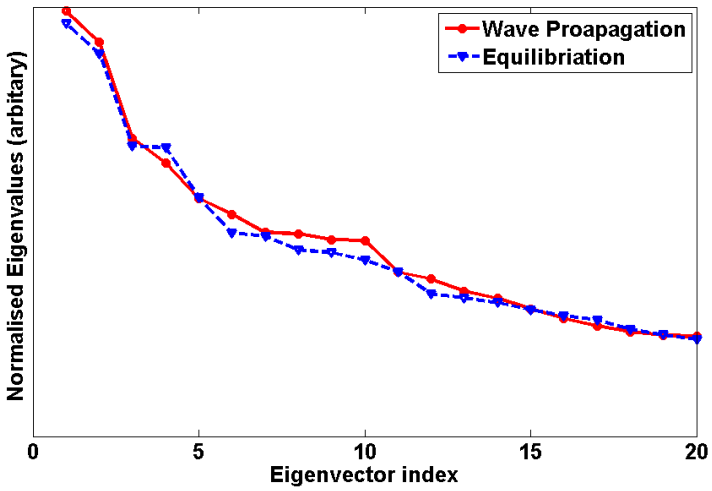

Fig. 13: Deflection modes excited by the acoustic flow obtained from principal component analysis.

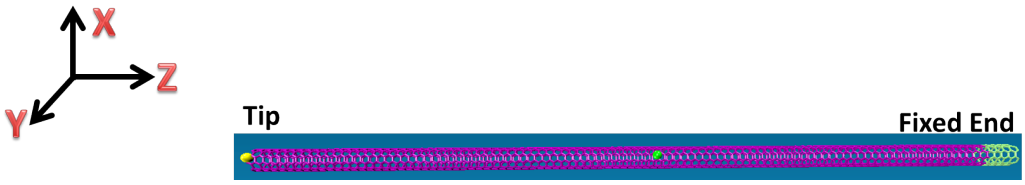

Fig. 14: CNT atom position to observe the displacement of the tip

contribution from random collisions with the surrounding argon molecules[18]. For the case with acoustic excitations, as shown in Figure 15b, the deflection in the direction transverse to the propagating wave, in the x-direction, is amplified considerably from its equilibrated position. It indicates that a portion of the acoustic energy contributes to amplifying the deflection of the CNT tip.

5. Conclusion

Based on the comparison of theoretical calculations and DSMC results to MD simulation results, the MD simulation of acoustic propagation in a standing wave tube with attenuation is believed to be validated. This means that the MD simulation method can be applied to understanding the sound field inside a standing wave tube with nanomaterials present. In addition, the behavior of a CNT in the presence of acoustic wave propagation in a monatomic gaseous media was studied. It was observed that the acoustic energy contributes to the CNT deflections. However, only a weak coupling exists between the CNT structure

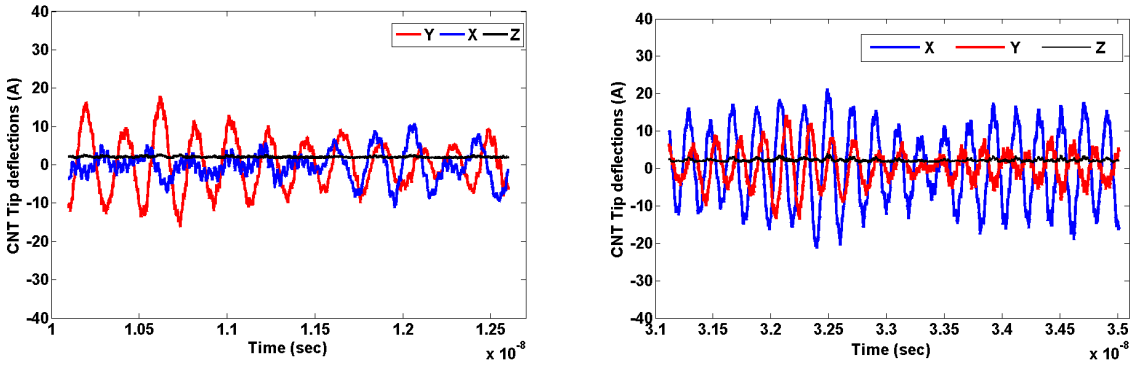

(a) **Without excitation** (b) **With excitation**

Fig. 15: CNT tip displacement, $d(x_i, y_i, z_i) = d_t - d_0(t = 0)$ **without** and **with excitation**. The atom position of the tip is shown in Figure 14.

and the propagating acoustic wave. This may be attributed to the differences of heat transfer rate of wave propagating media, i.e. argon gas being monatomic, and the CNT being polyatomic molecules. Based on the successful validation of the MD simulation of acoustic wave propagation against the DSMC results, it can be concluded that a platform has been developed to conduct MD simulation in the range of MHz frequency which would be beneficial to demonstrate the acoustic behavior of CNT. Overall, this study demonstrates the usefulness of MD simulation and the procedure that can be followed to study the acoustic absorption behavior of CNT.

Acknowledgement

This research was supported under Australian Research Council's Discovery Projects funding scheme (project number DP130102832). The authors would also like to acknowledge the financial support provided by the University of Adelaide through an International Postgraduate Research Scholarship (IPRS) and an Australian Postgraduate Award (APA). The assistance of Mr Jesse Coombs with the computational methods is greatly appreciated.

References

1. J. Czerwinska, Continuum and non-continuum modelling of nanofluidics, Technical Report 8, NATO Research and Technology Organisation, 2009, pp. 1-22.
2. A. D. Hanford, Numerical simulations of acoustics problems using the direct simulation monte carlo method, Phd thesis, The Pennsylvania State University, University Park, State College, PA 16801, United States, 2008.
3. N. G. Hadjiconstantinou, Sound wave propagation in transition-regime micro- and nanochannels, *Phys. Fluids* **14** (2002) 802 – 809.

4. G. Karniadakis, A. Beskok and N. R. Aluru, *Microflows and Nanoflows: Fundamentals and Simulation*, Indisciplinary Applied Mathmatics (Springer, New York, 2005).
5. M. Ayub, A. C. Zander, C. Q. Howard and B. S. Cazzolato, A review of acoustic absorption mechanisms of nanoscopic fibres, in *Proc. Acoustics'11* (Gold Coast, Australia, 2011), pp. 77 – 84.
6. M. Ayub, A. C. Zander, C. Q. Howard, B. S. Cazzolato and D. M. Huang, A review of md simulations of acoustic absorption mechanisms at the nanoscale, in *Proc. Acoustics'13* (Victor Harbor, Australia, 2013), pp. 19–26.
7. N. G. Hadjiconstantinou and A. L. Garcia, Molecular simulations of sound wave propagation in simple gases, *Phys. Fluids* **13** (2001) 1040 – 46.
8. L. L. Beranek and I. L. Ver, *Noise and Vibration Control Engineering: Principles and Applications* (John Wiley and Sons, New York, USA, 1992).
9. C. F. Carlborg, J. Shiomi and S. Maruyama, Thermal boundary resistance between single-walled carbon nano-tubes and surrounding matrices, *Phys. Rev. B* **78** (2008) 1 – 8.
10. J. D. Weeks, D. Chandler and H. C. Andersen, Role of repulsive forces in determining the equilibrium structure of simple liquids, *J. Chem. Phys.* **54** (1971) 5237–5247.
11. R. J. Wang and K. Xu, The study of sound wave propagation in rarefied gases using unified gas-kinretic scheme, *Acta Mech. Sinica* **28** (2012) 1022–1029.
12. S. Plimpton, Fast parallel algorithms for short-range molecular dynamics, *J. Comput. Phys.* **117** (1995) 1 – 19.
13. T. Yano, Molecular dynamics study of sound propaga-tion in a gas, in *AIP Conf. Proc.* (2012), volume 1474, pp. 75–78.
14. L. Sirovich and J. K. Thurber, Propagation of forced sound waves in rarefied gasdynamics, *J. Acoust. Soc. Am.* **37** (1965) 329.
15. M. Greenspan and M. C. Thompson, Jr., An eleven megacycle interferometer for low pressure gases, *J. Acoust. Soc. Am.* **25** (1953) 92.
16. D. W. Brenner, O. A. Shenderova, J. A. Harrison, S. J. Stuart, B. Ni and S. B. Sinnott, A second-generation reactive empirical bond order (rebo) potential energy expression for hydrocarbons, *J. Phys.: Condens. Matter* **14** (2002) 783.
17. C. Chen, M. Ma, K. Jin, J. Z. Liu, L. Shen, Q. Zheng and Z. Xu, Nanoscale fluid-structure interaction: Flow resistance and energy transfer between water and carbon nanotubes, *Phys. Rev. E* **84** (2011) 046314.
18. C. Chen and X. Zhiping, Flow-induced dynamics of carbon nanotubes, *Nanoscale* **3** (2011) 4383 – 4388.

Appendix

A. Effect of Thermostat

The effect of the thermostat is illustrated in Figure A.1. A comparison of the mean spatial gas temperature without and with NVT thermostats with varying damping times is presented in Figures A.1a and A.1b. As shown in Figure A.1a, without a thermostat this increase the gas temperature linearly with time, and with the inclusion of an NVT thermostat it can be controlled. However, thermostatting may also damp the oscillating pressure amplitude. Hence, it was necessary to ensure that the use of a thermostat does not affect the propagating wave. This was done by adjusting the thermostatting damping time (τ) as a function of the integer period of the acoustic frequency (ω), i.e. $\tau = n(\frac{2\pi}{\omega})$ with $n = 1, 2, ...$ As shown in Figure A.1b, strongly coupled thermostats with smaller damping

time of 1, 2 or 3 periods, affect the propagating wave. On the other hand, thermostats with larger damping times of 4, 5 and 10 periods, i.e. loosely coupled thermostats, can control the increasing temperature without damping the propagating wave as shown in Figures A.1a. It was observed that the damping time of 5 periods shows the best possible control of the temperature. Therefore, all higher frequency simulations were performed using an NVT thermostat with a damping time of 5 periods.

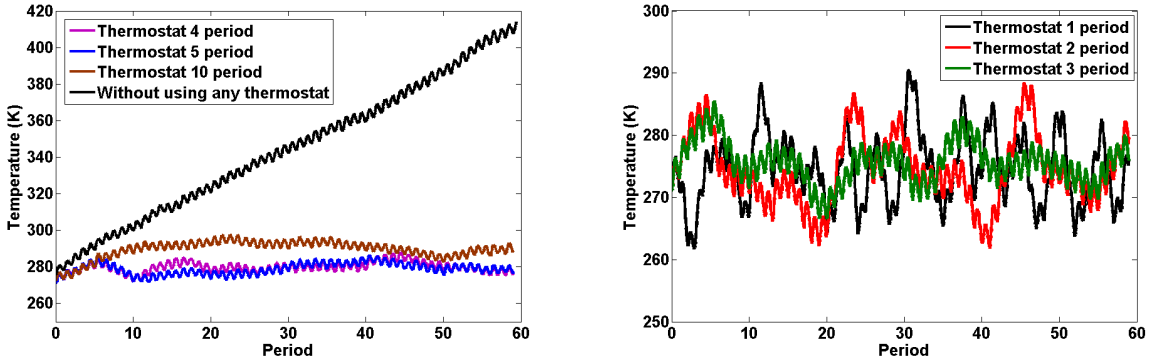

(a) Loosely coupled thermostat

(b) Strongly coupled thermostat

Fig. A.1: Variation of mean spatial gas temperature without and with NVT thermostats of varying damping times (a) 4, 5 and 10 periods and (b) 1, 2 and 3 periods. A thermostat with a damping time of 5 periods shows the best control of the temperature increase.